



HAL
open science

Neurovascular hypoxia trajectories assessed by photoacoustic imaging in a murine model of cardiac arrest and resuscitation

John Salvas, Katherine Leyba, Luke Schepers, Nitchawat Paiyabhroma, Craig Goergen, Pierre Sicard

► **To cite this version:**

John Salvas, Katherine Leyba, Luke Schepers, Nitchawat Paiyabhroma, Craig Goergen, et al.. Neurovascular hypoxia trajectories assessed by photoacoustic imaging in a murine model of cardiac arrest and resuscitation. IEEE Transactions on Ultrasonics, Ferroelectrics and Frequency Control, 2023, 10.1109/TUFFC.2023.3265800 . hal-04072363

HAL Id: hal-04072363

<https://hal.science/hal-04072363v1>

Submitted on 20 Jun 2023

HAL is a multi-disciplinary open access archive for the deposit and dissemination of scientific research documents, whether they are published or not. The documents may come from teaching and research institutions in France or abroad, or from public or private research centers.

L'archive ouverte pluridisciplinaire **HAL**, est destinée au dépôt et à la diffusion de documents scientifiques de niveau recherche, publiés ou non, émanant des établissements d'enseignement et de recherche français ou étrangers, des laboratoires publics ou privés.

Neurovascular hypoxia trajectories assessed by photoacoustic imaging in a murine model of cardiac arrest and resuscitation

John P. Salvas, Katherine A. Leyba, Luke E. Schepers, Nitchawat Paiyabhroma, Craig J. Goergen, and Pierre Sicard

Abstract— Cardiac arrest is a common cause of death annually mainly due to post cardiac arrest syndrome that leads to multiple organ global hypoxia and dysfunction after resuscitation. The ability to quantify vasculature changes and tissue oxygenation is crucial to adapt patient treatment in order to minimize major outcomes after resuscitation. For the first time, we applied high resolution ultrasound associated with photoacoustic imaging to track neurovascular oxygenation and cardiac function trajectories in a murine model of cardiac arrest and resuscitation. We report preservation of brain oxygenation is greater compared to that in peripheral tissues during arrest. Furthermore, distinct patterns of cerebral oxygen decay may relate to the support of vital brain functions. Additionally, we followed trajectories of cerebral perfusion and cardiac function longitudinally after induced cardiac arrest and resuscitation. Volumetric cerebral oxygen saturation decreased 24 hours post arrest, but these levels rebounded at one week. However, systolic and diastolic cardiac dysfunction persisted throughout and correlated with cerebral hypoxia. Pathophysiologic biomarker trends, identified via cerebral photoacoustic imaging in preclinical models, could provide new insights in understanding the physiopathology of cardiac arrest and resuscitation.

Index Terms— photoacoustic imaging, echocardiography, cardiac arrest, resuscitation

I. INTRODUCTION

Cardiac arrest is a common cause of death in the developed world and can be the result of various acute or chronic disease [1], [2]. Arrest is usually divided into in-hospital cardiac arrest (IHCA) and out-of-hospital cardiac arrest (OHCA) with varied outcomes and mortality for each type [1]. Although medical technologies have improved survivability of cardiac arrest and subsequent resuscitation, a great deal of patients will still experience a wide range of symptoms due to ischemic injury [3]. Long term consequences include neurodegeneration, fatigue, depression, cardiac hypokinesia, and overall decreased quality of life [4].

Recently, various clinical and preclinical studies have focused on outcomes after cardiac arrest [5]–[7]. A potentially important marker identified is cerebral oxygen saturation [8]. In human studies, near-infrared spectroscopy (NIRS) has been used to assess regional cerebral oxygenation [9]. Although NIRS is a useful tool for non-invasively measuring oxygenation in the superficial cerebral and cutaneous tissues, there are limitations such as skull thickness interference and the challenge of differentiating and precisely localizing NIRS signal changes in the brain or scalp [10].

Photoacoustic imaging (PAI) is an emerging technology with promising clinical translation. It is an imaging modality that combines the contrast and specificity of optical imaging with the high spatial resolution of ultrasound [11], [12]. Recently, it has gained more attention in the fields of cardiology and neuroscience due to its ability to characterize cardiac function in various disease states [13], [14] as well as the ability to image vasculature changes and tissue composition [11], [15]. Photoacoustic imaging is also able to image at greater depths compared to traditional optical imaging techniques [16]. In combination with ultrasound, photoacoustic imaging has been shown to correct artifacts generated by the

Manuscript submitted December 14, 2022. This work was supported by the Fulbright United States Scholars Program, the Montpellier Advanced Knowledge Institute on Transitions (MAKIT) Program of the Université de Montpellier, the French-American Cultural Exchange (FACE) Foundation, and the Chateaubriand Fellowship Program.

This work involved animal subjects in the protocol. The authors confirm that institutional review boards approved research procedures.

John Salvas, Katherine Leyba, Luke Schepers, and Craig Goergen are with Purdue University, Weldon School of Biomedical Engineering in the Cardiovascular Imaging Research Laboratory, 206 South Martin Jischke Dr,

West Lafayette, IN, USA, 47907 (email: jsalvas@purdue.edu, leybak@purdue.edu, lschepers@purdue.edu, and cgoerden@purdue.edu).

Nitchawat Paiyabhroma and Pierre Sicard are with the Institut national de la santé et de la recherche médicale (INSERM) and the centre national de la recherche scientifique (CNRS) in IPAM/PhyMedExp/Biocampus Laboratory at the Université de Montpellier, 371 Avenue du Doyen Gaston Giraud, 34000, Montpellier, France (email: paiyabhroma.nitchawat@inserm.fr, pierre.sicard@inserm.fr).

skull and can thus provide a better view of cortical microvasculature in mice [17]. The most commonly used optical wavelengths in PAI are visible and near-infrared (NIR) light, with 550 to 900 nm wavelengths [11]. Wavelengths in the second near-infrared window (NIR-II) ranging from 1000 to 1700 nm are currently being explored for preclinical and clinical applications because they offer greater depths of penetration and higher spatial resolution to better visualize structures deep within tissue [18]. The absorption spectra of tissue chromophores allows larger biomolecular structures to be probed with great specificity, so long as the probing light is tuned to the correct wavelength [19]. For example, 1100 nm has been used to target hemoglobin and 1210 nm to target lipid for atherosclerosis characterization in mice *in situ* [20]. Exogenous contrast agents have also been used to target atherosclerotic plaque biomarkers via intravascular PAI *ex vivo*, as demonstrated by Luke *et al.* [21].

For visualization of oxygen saturation, wavelengths of 750 nm and 850 nm can be used via a dual wavelength approach to target oxygenated and deoxygenated hemoglobin, respectively [22]. In murine models of myocardial infarction and mild traumatic brain injury, the use of PAI for monitoring oxygenation in the heart and brain as well as peripheral organs has been accomplished using this method [23], [24]. However, photoacoustic imaging has not been applied to assess brain oxygen trajectories during cardiac arrest and resuscitation. The ability to do so could provide insight into potential functional outcomes post-resuscitation such as hypoxic-ischemic brain injury, ischemic stroke, or cerebral hemorrhage [25].

Here, we implement a murine model of cardiac arrest with and without resuscitation and, for the first time, apply photoacoustic imaging and echocardiography to assess trends in neurovascular and cardiac function. In this study, PAI in mice was performed for up to one week to assess oxygen changes in the brain regionally and globally. Cardiac ultrasound imaging was also used up to one week and is complemented by recordings of electrocardiogram signals throughout the cardiac arrest and resuscitation procedure. Using this approach, we identify and quantify biomarkers such as oxygen saturation (sO_2), total hemoglobin (HbT), cardiac global longitudinal strain and ejection fraction, among others to determine correlation between neurological and cardiovascular parameters that may be useful in predicting functional outcomes from an imaging perspective.

II. METHODS

A. Animal Model

Experiments were performed following European Directive (2010/63/EU) and French laws governing laboratory animal use [26]. The investigation was approved by the local ethics committee (APAFIS #2019111811257350_v2). Swiss breeder mice were obtained through Janvier Labs (Le Genest-Saint-Isle, France). We maintained the animal habitat at a consistent $21^\circ\text{C} \pm 1^\circ\text{C}$ with humidity of $55\% \pm 1\%$. Mice were assigned to cardiac arrest without resuscitation ($n=5$) or with resuscitation ($n=10$).

B. Cardiac Arrest without Resuscitation

Animals were anesthetized using 2.5-3% isoflurane at 2.0 L/min and placed in prone position on an imaging stand

(FUJIFILM VisualSonics INC., Toronto, ON, Canada) with a heating pad. Body temperature was maintained at 37°C throughout the procedure. Electrocardiogram (ECG) subcutaneous needles were inserted into all extremities to monitor cardiac rhythm (eBox, FUJIFILM VisualSonics). We applied depilatory cream to the cranium to remove all hair. The head was immobilized, and centrifuged ultrasound gel was applied to the skull. We warmed the tail for 1 minute then inserted a 27-gauge tail vein cannula. The cannula was secured with tape. 2D photoacoustic images were acquired at frequency 4 Hz for the entire procedure. After obtaining baseline readings for 30 seconds, we injected 90 μL of 0.1 g/mL KCl into the tail vein followed by 10 μL of saline to flush the line. KCl was used as an arresting agent as a rapid increase in extracellular KCl disrupts cardiac myocyte resting membrane potential and inactivates fast sodium channels responsible for conduction of action potentials in the heart [27], [28]. The heartbeat stopped within 30 seconds on average, and we continued obtaining photoacoustic images for five minutes after the onset of asystole.

C. Cardiac Arrest with Resuscitation

In the cardiac arrest with resuscitation cohort, we obtained baseline three-dimensional (3D) cerebral photoacoustic images in addition to cardiac function assessed with 2D ultrasound, described below. The mice were then anesthetized as described and the body temperature was maintained at 37°C with a heating pad (Temperature control Unit HB101/2, Panlab, USA). In a supine position, a small incision was made on the neck to visualize the trachea. We intubated the animal and placed it on a ventilator (MiniVent Type 845, Hugo Sachs Elektronik, Germany) on room air and isoflurane with a respiratory rate of 140 breaths/min and a tidal volume of 225 μL . The tail vein was cannulated with a 27-gauge needle and line (Fig 1A). Electrode needles were inserted into two appendages to monitor ECG tracings throughout the procedure (Fig. 1B) (PowerLab 26T, ADInstruments, UK). Once the animal was stable, 50 to 60 μL of 0.1 g/mL KCl was injected into the tail vein followed by 10 μL saline to flush the line. We switched off the ventilation and waited for 6.5 minutes, at which point we resumed ventilation and started chest compressions at roughly 300 beats/min. We began a 1 mL infusion of 30 $\mu\text{g}/\text{mL}$ Adrenaline at a rate of 1 mL/min using an automatic syringe pump (Harvard Apparatus PHD 2000, Holliston, MA, USA). We stopped compressions once the heartbeat resumed or after 4 minutes. Three animals did not survive the procedure; thus, they were excluded from analysis. One mouse died 4-5 hours after resuscitation, and another died after 2 days lowering the sample sizes for follow-up imaging timepoints (Fig 1C).

D. Photoacoustic Imaging

PAI was performed with a Vevo 3100 high-frequency ultrasound system with a LAZR-X (Nd:YAG 680-2000 nm) add-on via a 21 MHz linear array transducer (MX250D; FUJIFILM VisualSonics). We anesthetized animals as previously described and placed them prone on an imaging stand. Depilatory cream was applied to the cranium to remove all hair. We immobilized the head and applied centrifuged ultrasound gel to avoid imaging artifacts from bubbles. 2D PAI

data was obtained at one coronal midbrain cross-section in the cardiac arrest without resuscitation cohort. Data was analyzed for decay parameters in the skin, the whole brain, and six specific regions of the brain: inferior, left inferior, right inferior, left superior, right superior, and superior.

In the cardiac arrest with resuscitation cohort, we recorded volumetric PAI data by horizontal stack scanning from the olfactory to occipital lobes of the brain using a linear stepper motor with approximately 90 slices per dataset. The imaging wavelengths were set to 750 and 850 nm, which correspond to oxygenated and deoxygenated hemoglobin, respectively [29], [30]. Acquisition parameters were set to an image depth of 20 mm, image width of 18 mm, a PA gain of 34 dB, a 2D gain of 23 dB, a hemoglobin threshold of 20, and a frame rate of 43 fps. Photoacoustic imaging was conducted at baseline, one hour, one day, and one week post arrest and resuscitation (Fig 1C). We analyzed images offline using Vevo LAB (v5.5.1, FUJIFILM VisualSonics) to obtain oxygen saturation (sO_2) and total hemoglobin (HbT) concentration measurements in the whole brain volume at each timepoint.

E. Cardiac Ultrasound Imaging

We used a Vevo 3100 high-frequency ultrasound system (FUJIFILM VisualSonics) with a 40 MHz centerline frequency

MX550D linear array probe to assess cardiac function. Mice were anesthetized as previously described and placed on an imaging stage in a supine position. We removed the ventral thorax hair with depilatory cream and applied ultrasound gel. We monitored respiratory rate and ECG tracings throughout the imaging process via the embedded electrodes within the stage.

Murine echocardiography was performed following American Physiological Society guidelines [31]. In a parasternal long-axis view, we quantified systolic function by obtaining measurements of left ventricular volumes, ejection fraction (EF), and both global and regional longitudinal strain. Diastolic function was assessed in a four-chamber view with measurements of mitral valve (MV) flow. Imaging was performed at baseline and three and seven days post cardiac arrest and resuscitation (Fig 1C). Vevo LAB Software v5.7.1 (FUJIFILM VisualSonics) was used for quantitative offline image analysis.

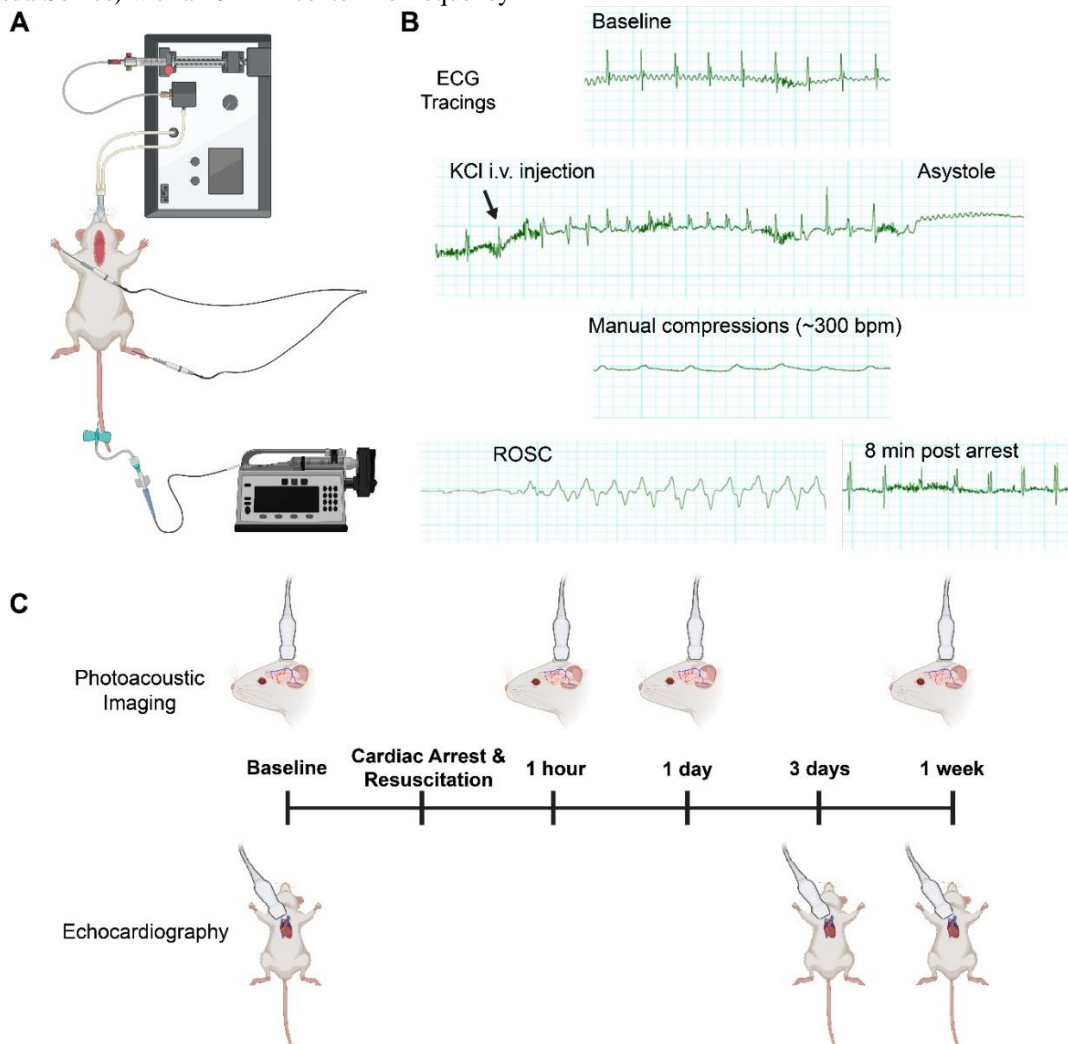


Figure 1. Experimental setup and study timeline (A) Cardiac arrest with resuscitation experimental setup. A small incision was made in the neck for intubation and the tail vein was cannulated for adrenaline injection during resuscitation. (B) The electrocardiogram (ECG) was recorded throughout the procedure from

baseline to the return of spontaneous circulation (ROSC) and onwards. (C) Photoacoustic and echocardiography imaging timeline in the cardiac arrest and resuscitation cohort. Image created with BioRender.com

F. Statistical Analysis

We used Prism 9.3 (GraphPad Software, San Diego, CA, USA) for all statistical analyses. The plateau followed by one-phase decay function was used to analyze oxygen saturation decay over time in the cardiac arrest without resuscitation cohort. The start time of decay was constrained in brain and skin and the regional cerebral analyses to ensure all decay functions began at the same time. A least squares regression with 1000 iterations for convergence was used to maximize the goodness of fit. Decay parameters of interest for each animal were baseline sO_2 , final or plateau sO_2 , and the time constant (τ), a measure of exponential decay rate. τ is defined as the time required to reach approximately 36.8% of the final steady state value from the onset of decay. It is found by calculating 62.8% of the difference between the baseline and final values which is then subtracted from baseline. All data including decay parameters, cardiac ultrasound, and cerebral PAI were compared using a one-way ANOVA with Tukey post hoc multiple comparison's test to investigate differences between cohorts.

Prior to Pearson Correlation, a Shapiro-Wilk test verified normality of all data. Cerebral sO_2 one day post arrest

measurements were correlated with cardiac function parameters three days post arrest. The correlation coefficient (r) and corresponding p -value are displayed. The threshold for statistical significance was set at $p < 0.05$, with levels of significance depicted as $p < 0.05^*$, $p < 0.01^{**}$, and $p < 0.001^{***}$. Data are presented as mean \pm standard deviation.

III. RESULTS

A. Structure and region-specific oxygen saturation decay profiles

We used PAI to evaluate and track structural and regional neurovascular oxygenation over time before, during, and after the onset of cardiac arrest (Fig 2A-C). At baseline, mean sO_2 was greater in brain compared to superficial cutaneous tissue and skin (brain 72.89 ± 4.36 , skin $56.94 \pm 8.69\%$, $p = 0.006$, Fig. 2D). After cardiac arrest, the oxygen saturation entered a plateau in which the brain tissue remained at a higher saturation level compared to the skin (Fig. 2E). The decay profile of brain tissue oxygenation, quantified by τ (τ), was slower than skin, although this difference did not reach significance ($p = 0.121$; Fig. 2F).

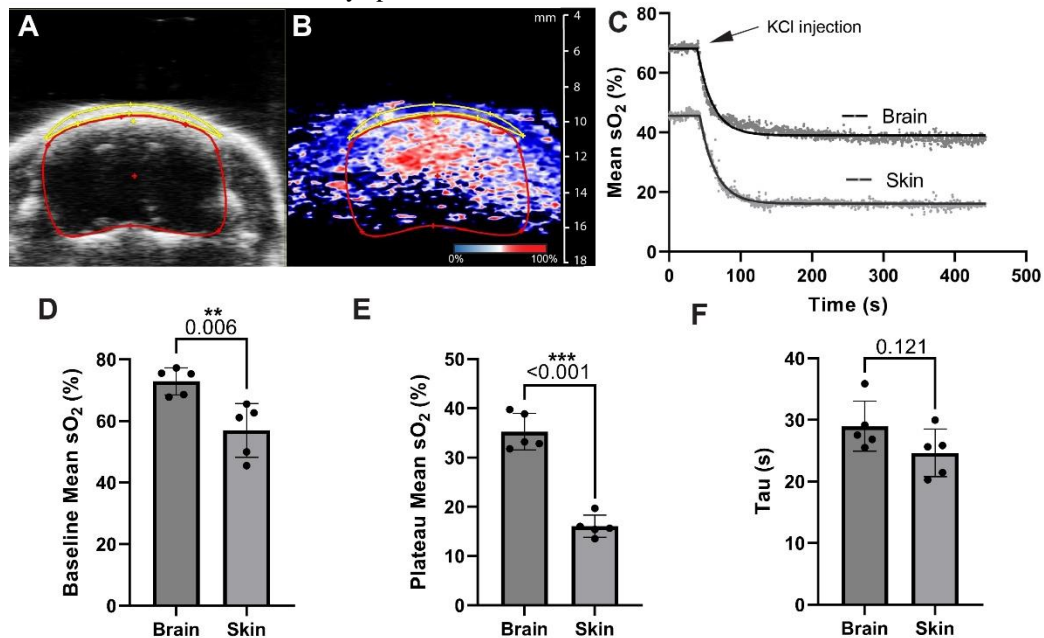


Figure 2. Photoacoustic imaging of the brain and skin. The structure of the cranium is seen in the (A) ultrasound on the upper left while the (B) photoacoustic measurements are seen on the right. The defined regions represent the areas used to assess skin (yellow) and brain (red) oxygenation. Color scaling shows regions of high sO_2 in red and regions of low sO_2 in blue/black. (C) Representative brain vs. skin oxygen saturation decay curve. (D) Baseline oxygenation, (E) plateau oxygenation, and (F) decay constant, τ , of the brain and skin. Sample size $n=5$. Results expressed as mean \pm SD.

PAI also allows for specific regional analyses. We investigated whether cardiac arrest elicits region-specific cerebrovascular sO_2 changes. The brain was divided into six regions (Fig. 3A-C). The inferior region encompasses the hypothalamic region of the brain while the superior regions capture cortical structures. At baseline, sO_2 levels did not differ between regions (Fig. 3D); however, the plateau phase sO_2 after arrest highlighted regional differences. The inferior regions plateau sO_2 was significantly higher than all superior regions.

Moreover, the inferior region's τ value was statistically greater than all other regions (Fig. 3E-F).

Next, we recorded cerebral oxygen saturation and hemoglobin levels in the acute and long-term using a novel cardiac arrest and subsequent resuscitation model. Volumetric PAI was employed to capture an average sO_2 that better represents the entire brain rather than one cross-section. Qualitative assessment of photoacoustic volumes shows the progression of a negative trend in saturation from baseline to

one hour, one day, and one week (Figure 4A-D; supplemental Figure 1). Interestingly, sO_2 maps at one hour depict similar levels to baseline; however, a region of desaturation is present in some animals at one day and persists to one week while

surrounding tissue returns to baseline oxygenation. These qualitative observations are quantified with no change between baseline and one-hour post resuscitation sO_2 (61.20 ± 4.99 vs. 55.32 ± 5.36 ; $p = 0.295$).

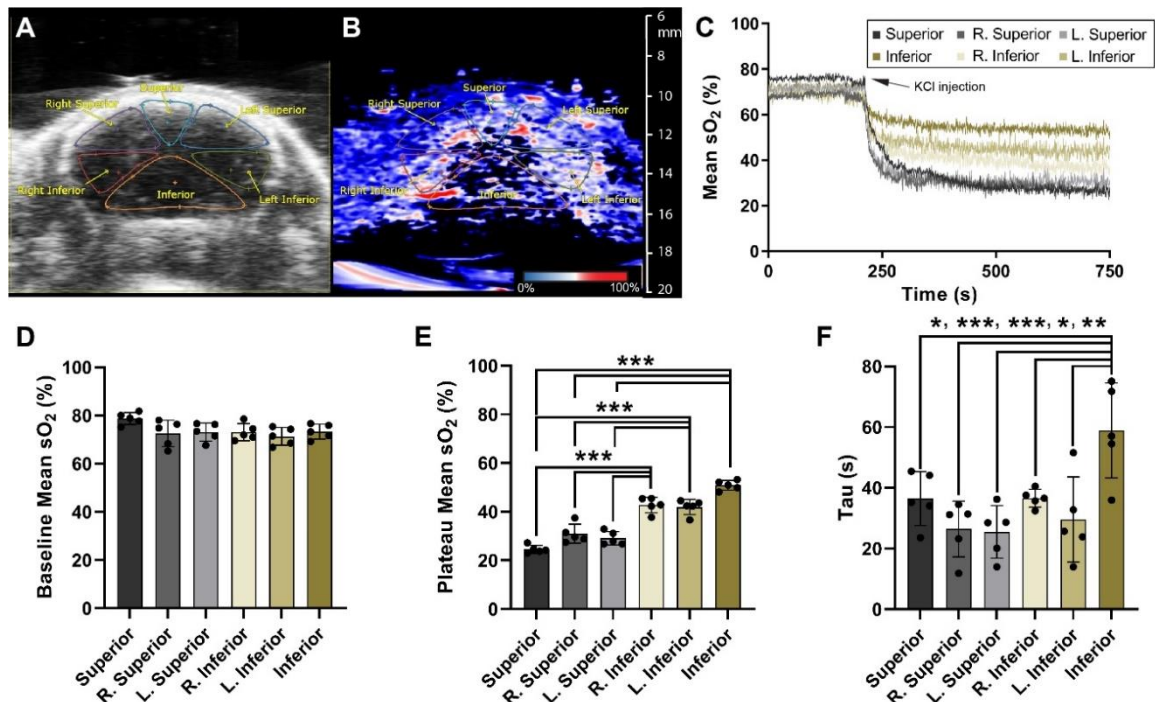


Figure 3. Regional photoacoustic imaging of the brain. The structure of the cranium is seen in the (A) ultrasound in the upper left while the (B) photoacoustic measurements are seen on the right. The six defined regions represent the areas used for sO_2 quantification. Color scaling shows regions of high sO_2 in red and regions of low sO_2 in blue/black. (C) Representative regional oxygen saturation decay curve. (D) Baseline, (E) plateau, and (F) decay constant, tau, of the six regions. Sample size $n=5$. Results expressed as mean \pm SD.

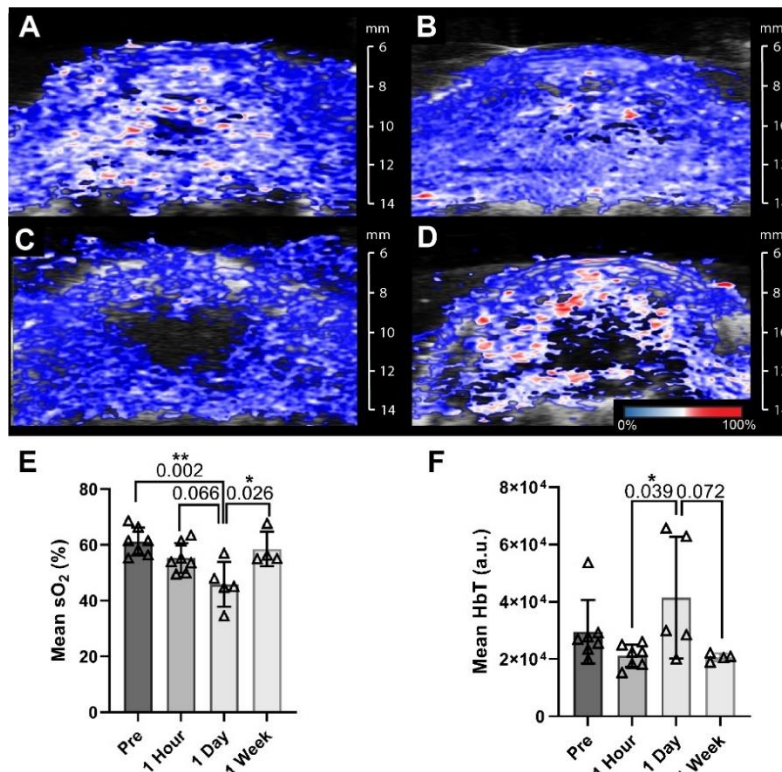


Figure 4. Neurovascular oxygenation trajectory with cardiac arrest and resuscitation. Representative cerebral oxygen saturation map at (A) baseline, (B) 1 hour, (C) 1 day, and (D) 1 week post arrest. Each image is from the same cross section of the 3D volume. Color scaling shows regions of high sO_2 in red and regions of low sO_2 in blue/black. (E) Volumetric mean sO_2 and (F) mean HbT over time. Results expressed as mean \pm SD.

At day one there was a significant drop in cerebral sO_2 (45.89 ± 8.03 , Fig. 4E) compared to baseline. Cerebral oxygen saturation returned to baseline levels one week post resuscitation. Cerebral HbT levels did not differ from baseline at one hour but show a significant increase from one hour to one day (2.11 ± 0.39 vs. $4.15 \pm 2.11 \times 10^4$; $p = 0.039$; Fig. 4E). Similar to oxygen saturation, HbT returned to levels comparable to baseline at one week.

B. Cardiac Function

To assess systolic and diastolic cardiac trajectories with arrest/resuscitation, we employed 2DUS at various timepoints (Fig. 1C). Global cardiac systolic function evaluated by ejection fraction decreased by nearly 10% from baseline to 3 days post arrest/resuscitation (63.17 ± 1.76 vs. 54.03 ± 4.59 , $p = 0.017$). While cerebral sO_2 levels returned to baseline at one-week, the ejection fraction remained decreased at one-week compared to baseline ($p = 0.012$, Fig. 5A). Global longitudinal strain showed a similar decrease from baseline at days 3 and one week, although no significant differences were seen (Fig. 5B).

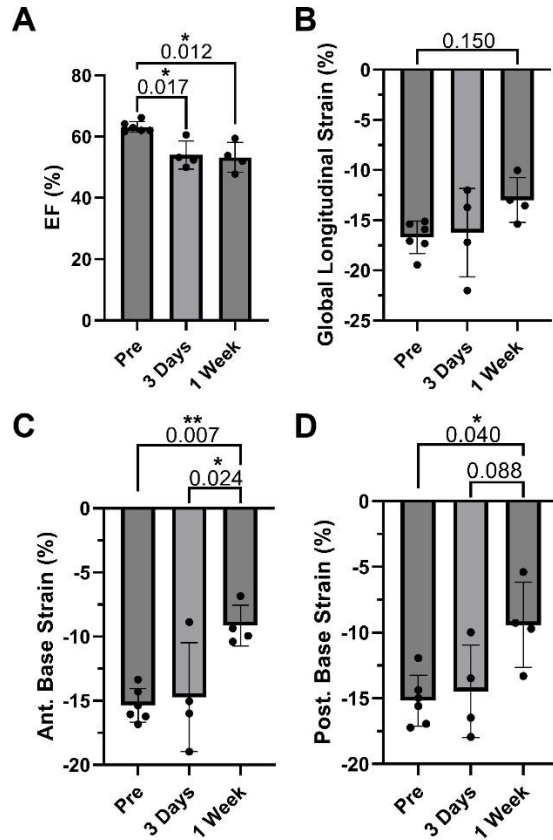


Figure 5. Systolic cardiac function pre and post cardiac arrest. (A) Ejection fraction, (B) global longitudinal strain, (C) anterior and (D) posterior basal longitudinal strains pre and post cardiac arrest. Results expressed as mean \pm SD.

Regional longitudinal strain analyses highlight specific motion abnormalities that may not be detectable by global metrics. The anterior basal regional strain significantly decreased from -15.65 ± 1.42 at baseline to -9.14 ± 1.58 at one-week (Fig. 5C). Posterior basal strain showed a similar trend to

anterior basal strain with a significant drop from baseline to one-week (-14.79 ± 2.03 vs. -9.42 ± 3.25 , $p = 0.040$, Fig 5D).

Cardiac diastolic function was evaluated with 2D ultrasound and flow through the mitral valve via Doppler ultrasound at the same timepoints (Fig. 6A). Quantitative metrics of interest were isovolumic relaxation time (IVRT), which measures the time from aortic valve closure to mitral valve opening [32], E/A ratio, which measures the ratio of peak blood flow in early to late diastole [33], and left atrial (LA) area. At 3 days, IVRT was increased compared to baseline (13.74 ± 1.20 vs 17.40 ± 2.19 , $p = 0.013$, Fig. 6B) which persisted to one week post arrest/resuscitation. The E/A ratio was within normal limits around 1.25 at baseline [34]. At 3 days, E/A ratio dropped below the normal range (0.96 ± 0.05 , $p = 0.018$) and remained below the normal limits at one-week, although this was not significant compared to baseline (1.03 ± 0.07 , Fig. 6C). Furthermore, LA area was increased three days after arrest ($p < 0.001$) and continued to increase to one week (Fig. 6D).

C. Cerebrovascular hypoxia correlates with cardiac systolic and diastolic dysfunction

Pearson correlation coefficients of non-invasive imaging biomarkers demonstrate an association between cerebral hypoxia and cardiac dysfunction post cardiac arrest. Cardiac systolic function assessed by EF three days post-arrest positively correlated with one-day cerebral sO_2 ($r = 0.993$, $p = 0.007$). Furthermore, volumetric cerebral sO_2 also positively correlated with the E/A ratio, a marker of diastolic function ($r = 0.978$, $p = 0.022$; Fig. 7A-B) [35].

IV. DISCUSSION

We demonstrate significant functional abnormalities in the brain and heart with mouse-specific correlations between cerebral hypoxia and cardiac dysfunction. Our data resonate with other studies implicating that cerebral oxygenation and cardiac dysfunction are important markers for assessing patients with cardiac arrest and subsequent resuscitation. Real-time monitoring of neurovasculature via photoacoustic imaging or other technologies has the potential to impact patient care.

A. Cardiac arrest elicits region-specific neurovascular oxygen saturation depletion

Vital organ perfusion is thought to be preserved in times of low oxygen availability [36]. The brain requires around 20% of the normal cardiac output and has the capacity to autoregulate blood flow to preserve tissue perfusion [37]. Mechanisms of autoregulation including smooth muscle regulation of vascular resistance have been investigated [38]; however, real-time global monitoring of this process in a model such as cardiac arrest has not been shown. We use PAI to monitor global and regional cerebral sO_2 decay profiles during cardiac arrest.

Our results confirm that vital organ blood flow is conserved with a slower decay profile in the brain as compared to subcutaneous tissue and skin (Fig. 2). More specifically in the brain, the inferior hypothalamic region displayed a slower saturation decay profile compared to cortical suggesting blood flow may be conserved in this region (Fig. 3). The

hypothalamus coordinates the endocrine system which includes vital regulation of blood pressure, heart rate, and body temperature [39]. Cortical regions, corresponding to the superior sections in Fig. 3, are more susceptible to ischemic damage [40], suggesting the mechanism of blood flow regulation may be associated with the profound neurologic effects of cardiac arrest including chronic fatigue, anxiety, depression, and decreased quality of life [41], [42]. Overall,

brain blood flow is preserved with low oxygen availability. We further show cerebral oxygenation is not distributed evenly and may be more preserved in regions responsible for homeostasis regulation (Fig. 3). Overall, neurovascular oxygen saturation decay during cardiac arrest displays regional-specific trajectories that may relate to vital functions.

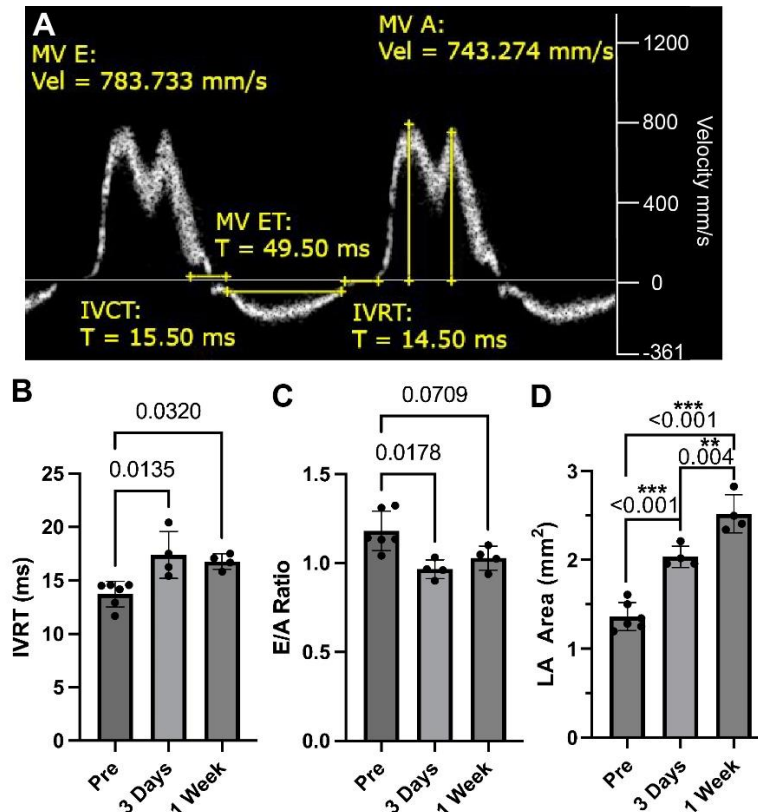


Figure 6. Diastolic cardiac function pre and post cardiac arrest. (A) Representative mitral valve flow tracing with measurements. MV E measures early mitral valve flow while MV A measures active phase flow. IVCT, IVRT and ET represent isovolumic contraction time, isovolumic relaxation time, and ejection time, respectively. (B) Isovolumetric relaxation time, (C) E/A ratio, and (D) LA area pre and post cardiac arrest. Results expressed as mean \pm SD.

B. Longitudinal cerebral perfusion following cardiac arrest

We also evaluated global cerebral sO_2 at baseline and followed animals up to one week post cardiac arrest and resuscitation. Cerebral sO_2 is an important clinical marker used in cardiac arrest patients to assess the severity of ischemic injury and potential outcomes [43]. Frontal lobe regional cerebral sO_2 measured immediately after arrest, assessed by near-infrared spectroscopy, has been shown to associate with long term neurologic outcomes [8], [44], suggesting that sO_2 measurements may offer insight into patient trajectories.

We captured a 3D volume of the brain to obtain an average volumetric sO_2 for whole brain perfusion quantification over time. Interestingly, we show that volumetric average sO_2 levels remained similar to baseline one hour post arrest and resuscitation but significantly dropped at twenty-four hours prior to returning to baseline at one week (Fig. 4). This finding highlights the progression of cerebral oxygenation illustrating functional differences may also persist after the initial injury. Mechanisms affecting the brain after ischemic episodes include ischemia-reperfusion injury, cerebral edema, and neuronal cell

death [45]–[48]. However, further work is needed to understand whether these mechanisms affect the observed global oxygen desaturation. Nonetheless, monitoring cerebral sO_2 immediately after arrest and longitudinally may offer further diagnostic and predictive value to patient care. Thus, these complex temporal patterns suggest cerebral perfusion levels fluctuate after cardiac arrest with a delayed onset, a finding that warrants further investigation of the brain and other organs.

C. Cardiac dysfunction progresses over time independent of neurovascular oxygenation

Manifestations of cardiac arrest effects are not isolated to the brain as cardiac systolic dysfunction and decreased cardiac output are seen acutely after arrest [49], [50]. We assessed cardiac function over time using high frequency 2DUS. We report significantly decreased ejection fraction three days and up to a week post arrest as well as abnormalities in regional cardiac strain. Additionally, cardiac diastolic function, assessed by IVRT, E/A ratio, and LA area, was decreased in conjunction

with systolic function over the same period (Fig. 6). Our work aligns with preclinical work by Rutledge *et al.* who show decreased ejection fraction one week post arrest and eventual recovery at four weeks [51]. Interestingly, cardiac dysfunction persists up to one week while cerebral oxygenation returns to baseline [51]. Thus, further work is needed to investigate the progression of long-term diastolic dysfunction after cardiac arrest and the mechanistic interplay between sustained cardiac dysfunction and neurovascular oxygenation.

D. Cerebral hypoxia associates with decreased cardiac function

Lastly, we correlated cerebral sO_2 with cardiac systolic and diastolic dysfunction parameters. Cerebral hypoxia one day post arrest correlated with ejection fraction and E/A ratio three days post arrest (Fig. 7). Work by David *et al.* in a myocardial infarction model highlight correlations between cardiac dysfunction and hypoxia in the brain, kidney, and liver [23]. Our results may further show this delicate interplay between cardiac dysfunction and peripheral organs; however, the limited sample size could affect the strength of correlation. A larger sample size in subsequent studies could confirm this tendency. Investigations into therapeutic targets on this axis have potential to improve cardiac and neurologic outcomes for patients after cardiac arrest.

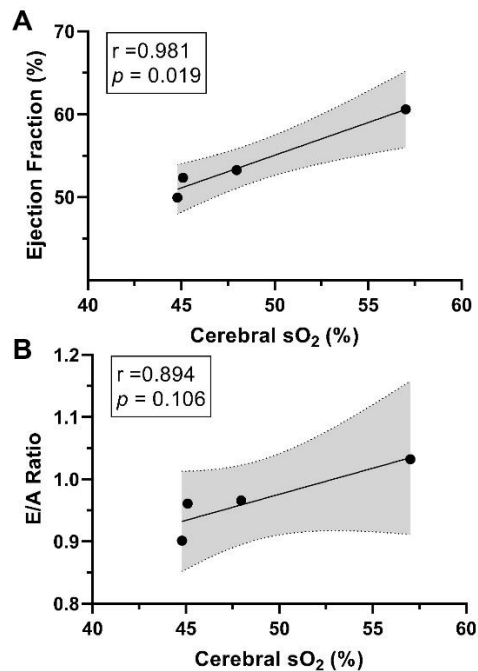


Figure 7. Relationship between cerebrovascular sO_2 and cardiac function. Pearson correlation between volumetric sO_2 1 day post cardiac arrest and (A) ejection fraction and (B) E/A ratio 3-days post cardiac arrest.

E. Limitations

The high spatial resolution, tissue quantification, and imaging depth permitted with PAI hold great promise for applications to cerebral imaging in humans [52]. The thickness of the human skull, around 8 mm, leads to strong signal attenuation and limits imaging directly to the cranial vault [52]. However, acoustic imaging windows through thinner regions of the skull (the temporal bone at 1 mm thick) or anatomical windows, including the nasal cavity and ocular region, have

promise in cerebrovascular evaluation in neurological surgery applications [53]. Continued development of these techniques and photoacoustic technologies could lead to further improvements in clinical applicability. Additionally, this study does not present histological analysis of tissue for evaluation of ischemic injury or molecular changes. Our functional assessments of both the brain and heart using PAI and echocardiography highlight trajectories after cardiac arrest that improve physiologic understanding and may have applicability to patient outcome evaluation. Histological and molecular changes will be investigated as a progression of our research.

V. CONCLUSION

In summary, PAI technology could be used to non-invasively evaluate global and regional cerebral sO_2 during cardiac arrest and resuscitation. We show that vital organ oxygenation is prioritized over peripheral tissues. More specifically, patterns of sO_2 vary by region, benefiting portions associated with vital function where higher sO_2 -levels were conserved. Furthermore, cerebral oxygen saturation rebounds in the hours after resuscitation, but may decline at 24 hours. Lastly, cardiac dysfunction persists to one week and dysfunction may associate with the cerebral sO_2 drop at one day. These findings suggest that continuous monitoring of functional abnormalities after cardiac arrest and their trajectories may have a clinical benefit.

APPENDIX

All data can be made available upon request.

ACKNOWLEDGMENT

We would like to acknowledge the animal housing staff at PhyMedExp and the Imagerie du Petit Animal de Montpellier (IPAM, Biocampus) for access to their high-resolution ultrasound and photoacoustic imaging equipment (LRQA Iso9001; France Life Imaging (grant ANR-11-INBS-0006); IBISA; Leducq Foundation (RETP), I-Site Muse).

Dr. Craig Goergen is a member of the FUJIFILM VisualSonics Inc. scientific advisory board. FUJIFILM VisualSonics had no role in study design, execution, or writing. All other authors declare no conflicts of interest.

REFERENCES AND FOOTNOTES

- [1] C. W. Tsao *et al.*, "Heart Disease and Stroke Statistics-2022 Update: A Report from the American Heart Association," *Circulation*, vol. 145, no. 8, pp. E153–E639, Feb. 2022, doi: 10.1161/CIR.0000000000001052/FORMAT/EPUB.
- [2] A. F. Sharabi and A. Singh, "Cardiopulmonary Arrest In Adults," *StatPearls*, Oct. 2022, Accessed: Nov. 13, 2022. [Online]. Available: <https://www.ncbi.nlm.nih.gov/books/NBK563231/>.
- [3] J. Elmer and C. W. Callaway, "The Brain after Cardiac Arrest," *Semin. Neurol.*, vol. 37, no. 1, p. 19, Feb. 2017, doi: 10.1055/S-0036-1597833.
- [4] R. W. Neumar *et al.*, "Post-Cardiac Arrest Syndrome," *Circulation*, vol. 118, no. 23, pp. 2452–2483, Dec. 2008, doi: 10.1161/CIRCULATIONAHA.108.190652.
- [5] R. Chocron *et al.*, "Ambulance density and outcomes after out-of-hospital cardiac arrest: Insights from the Paris sudden death expertise center registry," *Circulation*, vol. 139, no. 10, pp. 1262–1271, Mar. 2019, doi: 10.1161/CIRCULATIONAHA.118.035113/FORMAT/EPUB.

- [6] Y. B. Zhu, Y. Yao, Y. Ren, J. Z. Feng, and H. Bin Huang, "Targeted Temperature Management for Cardiac Arrest Due to Non-shockable Rhythm: A Systematic Review and Meta-Analysis of Randomized Controlled Trials," *Front. Med.*, vol. 9, Jun. 2022, doi: 10.3389/FMED.2022.910560.
- [7] B. S. Abella, D. Zhao, J. Alvarado, K. Hamann, T. L. Vanden Hoek, and L. B. Becker, "Intra-Arrest Cooling Improves Outcomes in a Murine Cardiac Arrest Model," vol. 109, pp. 2786–2791, 2004, doi: 10.1161/01.CIR.0000131940.19833.85.
- [8] N. Ito *et al.*, "Noninvasive regional cerebral oxygen saturation for neurological prognostication of patients with out-of-hospital cardiac arrest: A prospective multicenter observational study," *Resuscitation*, vol. 85, no. 6, pp. 778–784, 2014, doi: 10.1016/J.RESUSCITATION.2014.02.012.
- [9] P. W. McCormick, M. Stewart, M. G. Goetting, and G. Balakrishnan, "Regional cerebrovascular oxygen saturation measured by optical spectroscopy in humans," *Stroke*, vol. 22, no. 5, pp. 596–602, 1991, doi: 10.1161/01.STR.22.5.596.
- [10] M. Ferrari, L. Mottola, and V. Quaresima, "Principles, Techniques, and Limitations of Near Infrared Spectroscopy," <https://doi.org/10.1139/h04-031>, vol. 29, no. 4, pp. 463–487, 2011, doi: 10.1139/H04-031.
- [11] P. Beard, "Biomedical photoacoustic imaging," *Interface Focus*, vol. 1, no. 4, pp. 602–631, 2011, doi: 10.1098/RFSF.2011.0028.
- [12] Huabei Jiang, "Photoacoustic Tomography," *Photoacoust. Tomogr.*, pp. 1–284, Jan. 2014, doi: 10.1201/9781315213903/PHOTOACOUSTIC-TOMOGRAPHY-HUABEIJIANG.
- [13] H.-C. A. Lin *et al.*, "Characterization of Cardiac Dynamics in an Acute Myocardial Infarction Model by Four-Dimensional Optoacoustic and Magnetic Resonance Imaging," *Theranostics*, vol. 7, no. 18, pp. 4470–4479, 2017, doi: 10.7150/thno.20616.
- [14] I. Ivankovic *et al.*, "Volumetric optoacoustic tomography enables non-invasive in vivo characterization of impaired heart function in hypoxic conditions," vol. 9, p. 8369, 2019, doi: 10.1038/s41598-019-44818-8.
- [15] H. Yang *et al.*, "Soft ultrasound priors in optoacoustic reconstruction: Improving clinical vascular imaging," *Photoacoustics*, vol. 19, Sep. 2020, doi: 10.1016/J.PACS.2020.100172.
- [16] L. V. Wang, "Prospects of photoacoustic tomography," *Med. Phys.*, vol. 35, no. 12, p. 5758, 2008, doi: 10.1118/1.3013698.
- [17] S. V. Bodea and G. G. Westmeyer, "Photoacoustic Neuroimaging - Perspectives on a Maturing Imaging Technique and its Applications in Neuroscience," *Front. Neurosci.*, vol. 15, p. 333, Jun. 2021, doi: 10.3389/FNINS.2021.655247/BIBTEX.
- [18] P. K. Upputuri and M. Pramanik, "Photoacoustic imaging in the second near-infrared window: a review," *J. Biomed. Opt.*, vol. 24, no. 4, p. 040901, Apr. 2019, doi: 10.1117/1.JBO.24.4.040901.
- [19] J. Yao and L. V. Wang, "Photoacoustic microscopy," *Laser Photon. Rev.*, vol. 7, no. 5, pp. 758–778, Sep. 2013, doi: 10.1002/LPOR.201200060.
- [20] G. S. Sangha and C. J. Goergen, "Label-free photoacoustic and ultrasound imaging for murine atherosclerosis characterization," *APL Bioeng.*, vol. 4, no. 2, p. 026102, Apr. 2020, doi: 10.1063/1.5142728.
- [21] G. P. Luke, D. Yeager, and S. Y. Emelianov, "Biomedical applications of photoacoustic imaging with exogenous contrast agents," *Ann. Biomed. Eng.*, pp. 422–437, 2012, doi: 10.1007/s10439-011-0449-4.
- [22] J. Kim *et al.*, "Programmable Real-time Clinical Photoacoustic and Ultrasound Imaging System," *Sci. Reports 2016 61*, vol. 6, no. 1, pp. 1–11, Oct. 2016, doi: 10.1038/srep35137.
- [23] H. David *et al.*, "Experimental Myocardial Infarction Elicits Time-Dependent Patterns of Vascular Hypoxia in Peripheral Organs and in the Brain," *Front. Cardiovasc. Med.*, vol. 7, Jan. 2021, doi: 10.3389/fcvm.2020.615507.
- [24] K. Leyba *et al.*, "Neurovascular hypoxia after mild traumatic brain injury in juvenile mice correlates with heart-brain dysfunctions in adulthood," *Acta Physiol.*, p. e13933, Jan. 2023, doi: 10.1111/APHA.13933.
- [25] I. Migdady *et al.*, "Brain Injury and Neurologic Outcome in Patients Undergoing Extracorporeal Cardiopulmonary Resuscitation: A Systematic Review and Meta-Analysis," *Crit. Care Med.*, vol. 48, no. 7, pp. E611–E619, 2020, doi: 10.1097/CCM.0000000000004377.
- [26] N. P. du Sert *et al.*, "Reporting animal research: Explanation and elaboration for the arrive guidelines 2.0," *PLoS Biol.*, vol. 18, no. 7, Jul. 2020, doi: 10.1371/JOURNAL.PBIO.3000411.
- [27] M. A. B. de Oliveira, A. C. Brandi, C. A. dos Santos, J. L. L. Cortez, and D. M. Braile, "Modes of induced cardiac arrest: hyperkalemia and hypocalcemia -Literature review," *Rev. Bras. Cir. Cardiovasc.*, vol. 29, no. 3, p. 432, Jul. 2014, doi: 10.5935/1678-9741.20140074.
- [28] H. B. Fallouh, J. C. Kentish, and D. J. Chambers, "Targeting for cardioplegia: arresting agents and their safety," *Curr. Opin. Pharmacol.*, vol. 9, no. 2, pp. 220–226, Apr. 2009, doi: 10.1016/J.COPH.2008.11.012.
- [29] A. Needles *et al.*, "Development and initial application of a fully integrated photoacoustic micro-ultrasound system," *IEEE Trans. Ultrason. Ferroelectr. Freq. Control*, vol. 60, no. 5, pp. 888–897, 2013, doi: 10.1109/TUFFC.2013.2646.
- [30] Y. Y. Sun *et al.*, "Prophylactic Edaravone Prevents Transient Hypoxic-Ischemic Brain Injury: Implications for Perioperative Neuroprotection," *Stroke*, vol. 46, no. 7, pp. 1947–1955, Jul. 2015, doi: 10.1161/STROKEAHA.115.009162.
- [31] M. L. Lindsey, Z. Kassiri, J. A. I. Virag, L. E. De Castro Brás, and M. Scherrer-Crosbie, "Guidelines for measuring cardiac physiology in mice," *Am. J. Physiol. - Hear. Circ. Physiol.*, vol. 314, no. 4, pp. H733–H752, Apr. 2018, doi: 10.1152/ajpheart.00339.2017.
- [32] V. E. Smith, W. B. White, and M. K. Karimeddini, "Echocardiographic assessment of left ventricular diastolic performance in hypertensive subjects. Correlation with changes in left ventricular mass," *Hypertens. (Dallas, Tex. 1979)*, vol. 9, no. 2 Pt 2, pp. II-81–II-84, 1987, doi: 10.1161/01.HYP.9.2_PT_2.II81.
- [33] B. Johansson, F. Lundin, R. Tegerback, and L. Bojô, "E/a' ratio a simple detector of left ventricular dysfunction in patients with decreased ejection fraction," *Scand. Cardiovasc. J.*, vol. 52, no. 1, pp. 20–27, Jan. 2018, doi: 10.1080/14017431.2017.1414954.
- [34] S. Gao, D. Ho, D. E. Vatner, and S. F. Vatner, "Echocardiography in Mice," *Curr. Protoc. Mouse Biol.*, vol. 1, Mar. 2011, doi: 10.1002/9780470942390.MO100130.
- [35] S. S. Mitter, S. J. Shah, and J. D. Thomas, "A Test in Context: E/A and E/e' to Assess Diastolic Dysfunction and LV Filling Pressure," *J. Am. Coll. Cardiol.*, vol. 69, no. 11, pp. 1451–1464, Mar. 2017, doi: 10.1016/J.JACC.2016.12.037.
- [36] S. G. Sakka *et al.*, "Assessment of Regional Perfusion and Organ Function: Less and Non-invasive Techniques," *Front. Med. / www.frontiersin.org*, vol. 1, p. 50, 2019, doi: 10.3389/fmed.2019.00050.
- [37] M. J. Cipolla, "Control of Cerebral Blood Flow - The Cerebral Circulation," vol. Chapter 5, Morgan & Claypool Life Sciences, 2009.
- [38] J. Duffin, D. J. Mikulis, and J. A. Fisher, "Control of Cerebral Blood Flow by Blood Gases," *Front. Physiol.*, vol. 12, p. 122, Feb. 2021, doi: 10.3389/FPHYS.2021.640075/BIBTEX.
- [39] Z. Shahid, E. Asuka, and G. Singh, "Physiology, Hypothalamus," in *Physiology, Treasure Island (FL): StatPearls Publishing, 2022*.
- [40] G. Hagberg, H. Ihle-Hansen, E. C. Sandset, D. Jacobsen, H. Wimmer, and H. Ihle-Hansen, "Long Term Cognitive Function After Cardiac Arrest: A Mini-Review," *Front. Aging Neurosci.*, vol. 14, 2022, doi: 10.3389/fnagi.2022.885226.
- [41] E. M. Wachelder, V. R. M. P. Moulart, C. van Heugten, J. A. Verbunt, S. C. A. M. Bekkers, and D. T. Wade, "Life after survival: long-term daily functioning and quality of life after an out-of-hospital cardiac arrest," *Resuscitation*, vol. 80, no. 5, pp. 517–522, May 2009, doi: 10.1016/J.RESUSCITATION.2009.01.020.
- [42] D. Naber and M. Bullinger, "Psychiatric sequelae of cardiac arrest," *Dialogues Clin. Neurosci.*, vol. 20, no. 1, Apr. 2018, doi: 10.31887/DCNS.2018.20.1/dnaber.
- [43] C. Storm *et al.*, "Regional cerebral oxygen saturation after cardiac arrest in 60 patients—a prospective outcome study," *Resuscitation*, vol. 85, no. 8, pp. 1037–1041, 2014, doi: 10.1016/J.RESUSCITATION.2014.04.021.
- [44] W. J. Joo *et al.*, "Prediction of the neurological outcome using regional cerebral oxygen saturation in patients with extracorporeal cardiopulmonary resuscitation after out-of-hospital cardiac arrest: a multicenter retrospective cohort study," *Acute Med. Surg.*, vol. 7, no. 1, p. e491, Jan. 2020, doi: 10.1002/AMS2.491.
- [45] A. Sugita *et al.*, "Systemic impact on secondary brain aggravation due to ischemia/reperfusion injury in post-cardiac arrest syndrome: a

prospective observational study using high-mobility group box 1 protein,” *Crit. Care*, vol. 21, no. 247, 2017, doi: 10.1186/s13054-017-1828-5.

- [46] H. K. Eltzschig and C. D. Collard, “Vascular ischaemia and reperfusion injury,” *Br. Med. Bull.*, vol. 70, no. 1, pp. 71–86, 2004, doi: 10.1093/bmb/ldh025.
- [47] Z. Dostovic, E. Dostovic, D. Smajlovic, O. C. Ibrahimagic, and L. Avdic, “Brain Edema After Ischaemic Stroke,” *Med. Arch.*, vol. 70, no. 5, pp. 339–341, 2016, doi: 10.5455/medarh.2016.70.339-341.
- [48] P. Rahaman and M. R. Del Bigio, “Histology of Brain Trauma and Hypoxia-Ischemia,” *Acad. Forensic Pathol.*, vol. 8, no. 3, p. 539, Sep. 2018, doi: 10.1177/1925362118797728.
- [49] G. Babini, K. Ameloot, and M. B. Skrifvars, “Cardiac function after cardiac arrest: what do we know?,” *Minerva Anesthesiol.*, vol. 87, no. 3, pp. 358–367, Mar. 2021, doi: 10.23736/S0375-9393.20.14574-7.
- [50] J. C. Jentzer, M. D. Chonde, and C. Dezfulian, “Myocardial Dysfunction and Shock after Cardiac Arrest,” 2015, doi: 10.1155/2015/314796.
- [51] C. A. Rutledge, T. Chiba, K. Redding, C. Dezfulian, S. Sims-Lucas, and B. A. Kaufman, “A novel ultrasound-guided mouse model of sudden cardiac arrest,” *PLoS One*, vol. 15, no. 12, p. e0237292, Dec. 2020, doi: 10.1371/JOURNAL.PONE.0237292.
- [52] B. Liang, S. Wang, F. Shen, Q. H. Liu, Y. Gong, and J. Yao, “Acoustic impact of the human skull on transcranial photoacoustic imaging,” *Biomed. Opt. Express*, vol. 12, no. 3, p. 1512, Mar. 2021, doi: 10.1364/BOE.420084.
- [53] M. T. Graham, J. Huang, F. X. Creighton, and M. A. Lediju Bell, “Simulations and human cadaver head studies to identify optimal acoustic receiver locations for minimally invasive photoacoustic-guided neurosurgery,” *Photoacoustics*, vol. 19, Sep. 2020, doi: 10.1016/J.PACS.2020.100183.



John Salvias has been a researcher in the Cardiovascular Imaging Research Lab at the Weldon School of Biomedical Engineering for a number of years. After earning his BS in Biomedical Engineering from Purdue University in December 2021, he interned with the Institut National de la Santé et de la Recherche Médicale (INSERM) in Montpellier, France. In the

future, he plans to pursue a medical degree.



Katherine Leyba received her BS in Electrical Engineering and BS in Biomedical Engineering from California State University, Long Beach in 2018. She is currently a PhD candidate in Biomedical Engineering at Purdue University in the Cardiovascular Imaging Research Laboratory. Katherine’s research interests include photoacoustics, ultrasound, cardiovascular imaging, deep learning, and image processing.



Luke Schepers received his BE in Mechanical Engineering from the University of Dayton in 2019. He is currently a PhD candidate in Biomedical Engineering at Purdue University in the Cardiovascular Imaging Research Laboratory. His research interests focus on medical imaging, cardiovascular disease, and cardiovascular devices.



Nitchawat Paiyabhroma received a PhD in cardiovascular physiology and photoacoustic imaging from the University of Montpellier in 2022. He holds an assistant professor position at Naresuan University (Thailand).



Craig Goergen is the Leslie A. Geddes Associate Professor of Biomedical Engineering at Purdue University. He is also the Director of Clinical programs in the Weldon School of Biomedical Engineering and an Adjunct Associate Professor of Surgery at Indiana University School of Medicine. Dr. Goergen holds a BS in Biomedical Engineering from Washington University in St. Louis and MS and PhD degrees in Bioengineering from Stanford University. Dr. Goergen joined the faculty at Purdue University in December of 2012.



Pierre Sicard is a research engineer at the Institut National de la Santé et de la Recherche Médicale (INSERM) in Montpellier, France. He is also in charge of the ultrasound/photoacoustic facility at IPAM. Dr. Sicard holds a PhD degree in Cardiovascular physiology from University of Burgundy (France) and did a post-doctoral position at King’s College London. Dr. Sicard joined INSERM in January 2016.